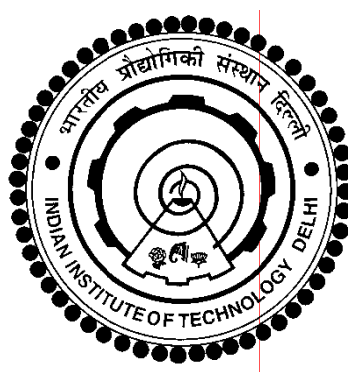


PROTEINS IN CROWDING AND CONFINEMENT

ASHIMA MALIK



DEPARTMENT OF CHEMISTRY
INDIAN INSTITUTE OF TECHNOLOGY DELHI
JANUARY 2016

©Indian Institute of Technology Delhi (IITD), New Delhi, 2016

PROTEINS IN CROWDING AND CONFINEMENT

by

ASHIMA MALIK

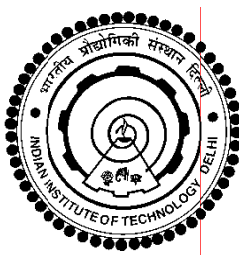
Department of Chemistry

Submitted

in fulfilment of the requirements of the degree of

Doctor of Philosophy

to the



Indian Institute of Technology Delhi

January 2016

*DEDICATED
TO
MY GRANDFATHER*

Late Ch. Mukhtiar Singh Malik

CERTIFICATE

This is to certify that the thesis titled “**Proteins in Crowding and Confinement**” being submitted by **Ms. Ashima Malik** to the **Indian Institute of Technology Delhi**, for the award of degree of **Doctor of Philosophy** is a record of bonafide research work carried out by her. **Ms. Ashima Malik** has worked under my guidance and supervision and has fulfilled the requirements for the submission of this thesis, which to my knowledge has reached the requisite standard.

The results contained in this thesis are original and have not been submitted, in part or full, to any other University or Institute for the award of any other degree or diploma.

Dr. Pramit K. Chowdhury

Associate Professor of Chemistry

Department of Chemistry

Indian Institute of Technology Delhi,

Hauz Khas, New Delhi- 110016

ACKNOWLEDGEMENTS

*The personality I am most indebted to is my research supervisor **Dr. Pramit K. Chowdhury**, who inculcated in me the spirit of scientific inquiry. Each and every discussion with him provided new insights on the subject of my study and could only strengthen my resolve to understand it better. He made learning and research most enjoyable by motivating discussions and by asking interesting questions. His communication skills, leadership qualities and integral view on research and his mission for providing 'only high-quality work and not less', has left a deep impression on my mind. When I was struggling, he constantly encouraged me not to give up. I also thank him for suggesting numerous improvements in this thesis.*

I would also like to thank all the past and present heads of the departments of Chemistry at IIT Delhi for providing me necessary facilities required for the completion of this research work.

I am thankful for the financial support provided by UGC as a Junior and Senior Research Fellowship over a period of 5 years.

This thesis would be incomplete without words of gratitude to all my lab members who helped me to make this thesis possible. To begin with, I would like to thank my labmates Jayanta, Saikat, Sanjib, Priyanka, Sandip, Saurabh and all the M.Sc. students who did project in my lab to provide a convivial place to work. Their kind support and guidance have been of great value in this work. I am also extremely grateful for the help given by Prof. A.K. Ganguly, Dr. Shashank Deep, Dr. Sameer Sapra and Dr. Nagendran for allowing me to use their instruments at the need of time. I would also like to thank their

students for always being supportive to me. The non teaching staff of the Instrumentation Laboratory of Chemistry Department also deserves special mention.

I would like to give a special thanks to my dear friends Preeti and Sanjib for always motivating me whenever I was depressed during the research period. A line of appreciation of course goes to some of my dearest friends Anu, Anil, Deepak, Vipul, Ankita, Sonam, Nisha, Gayatri, Rewa, Sarul, Kuldeep, Rahul and all my batchmates for their invariable support and indispensable help in achieving this feat.

I am deeply indebted to my family for their unflagging love, patience and support throughout my life, this dissertation is simply impossible without them. I put my deepest sense of regards and gratefulness to my father Mr. Azad Singh Malik and mother Mrs. Phoolwati Malik for their true blessings. I would like to offer a special thanks to my brother Ajay Malik and his wife Pooja for their moral support and invaluable advice during some of the most difficult and demanding moments of my life. I can't miss thanking my fiancé Anand Arya (to whom I will be married very soon) for his love, support and endurance.

I also thank my tauji Sh. Surajbhan Malik and Rajendra Malik and my cousin brothers Satish and Rajesh Malik for their love and support. My sincere apologies to those whom I could not mention due lack of space, but thank them equally.

Finally, and most important, I would like to thank the almighty GOD, for it is under his grace that we live, learn and flourish. May your name be exalted, honored, and glorified.

Ashima Malik

ABSTRACT

The thesis entitled “*Proteins in Crowding and Confinement*” focuses on the understanding of the effect of macromolecular crowding and confinement on the folding and unfolding of proteins and their differential effects on the respective conformational ensembles. The thesis features detailed investigation of the unfolding of two model proteins by thermal and/ or chemical denaturation means in presence of different macromolecular crowders utilizing various spectroscopic techniques.

The thesis has been divided into seven chapters.

Chapter I titled “**Introduction**” provides brief introduction to the phenomena of macromolecular crowding and confinement and their influence on the protein folding and unfolding. It also describes the objectives of the studies carried out in the thesis and the strategy devised to achieve the same. An effort has been made to present an overview of crowding and confinement studies that have been studied during the past years.

Chapter II titled “**Materials and Methods**” describes chemical procurement, purification and storage along with techniques used during the investigation. Specifically, steady-state and time-resolved fluorescence, UV-VIS spectroscopy, Circular Dichroism (CD) and Dynamic light scattering (DLS) measurements were used to carry out the requisite characterization. The techniques of fluorescence (steady-state and time-resolved) and CD spectroscopy have been employed to study the conformational changes of the proteins in confinement.

Chapter III titled “**Myoglobin unfolding in Crowding and Confinement**” includes a detailed investigation of the unfolding of the heme protein myoglobin (Mb) in presence of macromolecular crowders (Ficoll 70, Dextran 70 and Dextran 40) and in a confined (AOT reverse micelles in Isooctane (IO)) environment. Our results reveal that confinement effect can be quite destabilizing in nature for Mb with the extent of distortion depending on various factors such as water localized in the microemulsion water pools having different properties than bulk water and/or the interaction of Mb with the charged interfacial wall of AOT reverse micelle apart from the effects that are purely confinement related . Effects of the crowding agents on myoglobin show a deviation from the general notion that synthetic macromolecular crowding agents are always stabilizing in nature. Ficoll 70 was observed to be particularly destabilizing in its influence on Mb unfolding which indicates that effect of macromolecular crowders can be quite protein specific.

Chapter IV titled “**Interaction of ANS with Human Serum Albumin under Confinement: Important insights and relevance**” focuses on the conformational disposition of the multidomain protein HSA (585 amino acids) within the confinement of water pools of AOT reverse micelles and its interaction with a commonly used fluorescence probe 1-anilinonaphthalenesulfonate (ANS) inside the water pools. Our study reveals the presence of little or no interaction between HSA and ANS inside the AOT water pools which is expected based on the observed distortion of the protein secondary structure on reverse micelle entrapment, the latter resulting in disruption of the binding pockets available to ANS. These observations are in sharp contrast to what has been alluded to earlier wherein such probes have been hypothesized to bind to the well-defined binding cavities (e.g. subdomain IIA) that this serum albumin possesses.

Chapter V titled “**Dramatic Effects of Macromolecular Crowders on Drug Binding to Serum Albumins: Consequences and Physiological Relevance**” lays out a detailed investigation of drug binding to the serum proteins, HSA and BSA in presence of a series of macromolecular crowding agents, Dextran 6, Dextran 40, Dextran 70 and Ficoll 70, using the fluorescence probe Coumarin-153 as a representative drug molecule. Since crowding agents can modulate protein structures (both shape and size) in the native and denatured states, these would then also be expected to affect the ligand binding properties of such proteins. Collectively our results provide important insights into the mechanism by which the cellular interior can modulate the binding aspects of proteins, starting from the number of pockets available (hence increasing the transfer yield per protein) to changes in the binding affinity, the latter being very important for release of bound species.

Chapter VI titled “**Urea induced unfolding of Human Serum Albumin in presence of Macromolecular Crowders using Prodan as an extrinsic probe**” provides a detailed investigation of the unfolding behavior of the protein as a function of urea in presence of different macromolecular crowders by probing with the help of Prodan. Our data provide an in-depth analysis of how domain II of HSA gets perturbed in presence of the synthetic crowding agents by using intrinsic (Trp) and extrinsic (Prodan) probes, the latter being non-covalently bound. We conclude that the crowding agents provide significant modulation of the HSA structure, the latter depending on the type of excluded volume that the crowders exude.

Chapter VII titled “**Conclusions and Future Prospects**” presents the conclusions drawn from the overall investigation, starting from the conformational dispositions of proteins in crowded and confined environments to how the native state ligand binding properties can get

affected by macromolecular crowders. This thesis opens the door to a host of future research possibilities that will contribute significantly to the fundamental understanding of crowding and confinement.

TABLE OF CONTENTS

Title	Page
Certificate	i
Acknowledgements	ii
Abstract	iv
List of Figures	viii
List of Tables	xv
Chapter I: Introduction	
1.1 Introduction to Protein Folding	1
1.2 Macromolecular crowding	2
1.2.1 Introduction to Macromolecular Crowding	2
1.2.2 Effects of Macromolecular Crowding on Structure and Function of Biomolecules	6
1.2.3 Importance of Macromolecular Crowding	12
1.2.4 Macromolecular Crowding Agents	14
1.3 Confinement	18
1.3.1 Introduction to Confinement	18
1.3.2 Effect of Confinement on Biomolecules	20
1.3.2.1 Simulation Studies	20
1.3.2.2 Experimental studies	23
1.3.2.3 Ribosomal Confinement	24
1.3.3 Model System: Reverse Micelles	26
1.4 Proteins Used	29
1.4.1 Myoglobin	29
1.4.2 Serum Albumin Proteins	31
1.5 References	36
Chapter II: Experimental Methods and Materials	
2.1 Materials and methods	56
2.1.1 Materials	56
2.2 Spectroscopic measurements	57
2.2.1 Absorption spectroscopy	57
2.2.2 Steady state fluorescence spectroscopy	59
2.2.3 Time Resolved Fluorescence Spectroscopy	65
2.2.4 Time Resolved Fluorescence Anisotropy	78
2.2.5 Circular Dichroism measurements	81
2.2.6 Dynamic Light Scattering (DLS)	85

2.3 References	87
Chapter III: Myoglobin Unfolding in Crowding and Confinement	
3.1 Introduction	90
3.2 Materials and Methods	93
3.2.1 Preparation of protein solutions	94
3.2.2 Steady State Fluorescence	95
3.2.3 Circular Dichroism	95
3.2.4 Time resolved Fluorescence	97
3.2.5 DLS Measurements	98
3.3 Results and Discussion	98
3.3.1 Myoglobin (Mb) unfolding in confinement	98
3.3.2 Myoglobin unfolding in presence of macromolecular crowders	109
3.4 Summary and Conclusions	117
3.5 References	121
Chapter IV: Interaction of ANS with Human Serum Albumin under Confinement: Important insights and relevance	
4.1 Introduction	129
4.2 Experimental Section	132
4.2.1 Materials and methods	132
4.2.2 Preparation of protein solutions	133
4.2.3 Steady State Fluorescence	133
4.2.4 Circular Dichroism	134
4.2.5 Time resolved Fluorescence	134
4.3 Results and Discussion	137
4.3.1 Thermal denaturation	137
4.3.2 Fluorescence studies	141
4.3.3 Interaction of ANS with HSA	143
4.3.4 Time resolved Fluorescence and FRET Studies	147
4.3.5 Anisotropy Studies	157
4.4 Conclusion	162
4.5 References	164
Chapter V: Dramatic Effects of Macromolecular Crowders on Drug Binding to Serum Albumins: Consequences and Physiological Relevance	
5.1 Introduction	170
5.2 Experimental Section	171
5.2.1 Materials and Methods	171
5.2.2 Preparation of Solutions	172
5.2.3 Absorbance measurements	172
5.2.4 Fluorescence Measurements	173
5.3 Results and Discussion	173

5.3.1 Binding Stoichiometry using Job's Plot	173
5.3.2 Determination of Dissociation Constants	178
5.4 Conclusions	186
5.5 References	187
CHAPTER VI: Urea induced unfolding of Human Serum Albumin in presence of Macromolecular Crowders using Prodan as an extrinsic probe	
6.1 Introduction	190
6.2 Materials and Methods	191
6.2.1 Fluorescence Measurements	192
6.2.2 Chemical denaturation studies	194
6.3 Results	195
6.3.1 Steady State measurements	195
6.3.2 Time resolved fluorescence measurements	205
6.4 Discussion	212
6.5 Conclusion	218
6.6 References	219
CHAPTER VII: Summary and Future direction	223
ANNEXURE I : Supplementary Information for Chapter III	228
ANNEXURE II: Supplementary Information for Chapter IV	234
ANNEXURE III: Supplementary Information for Chapter V	245
ANNEXURE I V: Supplementary Information for Chapter VI	249
Brief Bio-Data of the Author	267

LIST OF FIGURES

	Page
Figure 1.1:	The nascent-peptide exit tunnel in the large ribosomal subunit. 1
Figure 1.2:	Representation of eukaryotic cytoplasm. The test protein molecule (<i>red</i>) is in a fluid medium that is crowded by soluble proteins (<i>green</i>), RNA species (<i>yellow</i>), and ribosomes (<i>pink</i>) and confined by cytoskeletal fibers (<i>blue</i>). 4
Figure 1.3:	Schematic representation of differences in excluded (<i>pink</i> and <i>black</i>) and available (<i>blue</i>) volume in a solution of spherical background macromolecules. <i>A</i> , volume available to a test molecule of infinitesimal size; <i>B</i> , volume available to a test molecule of size comparable with background molecules. 4
Figure 1.4:	Schematic representation of protein folding in presence of macromolecular crowding. 5
Figure 1.5:	Human immunodeficiency virus type 1 protease (HIVpr) in closed and open conformations, in the presence of crowder molecules. 7
Figure 1.6:	Structure of Dextran. 15
Figure 1.7:	Structure of Ficoll 70. 15
Figure 1.8:	Structure of PEG. 16
Figure 1.9:	Structure of PVP. 17
Figure 1.10:	Effect of confinement on configurational state of native (N) and unfolded state (U). Configuration (a) is not feasible because the protein chain crosses the boundary while the configuration (b) is allowed. Protein with spherical shape in native state cannot be located in position c but can be in position d. 19
Figure 1.11:	(A) Structure of sodium bis(2-ethylhexyl) sulfosuccinate (AOT). The surfactant head group is on the left of the red line and the tail is on the right of the red line. (B) Structure of a reverse micelle. 28
Figure 1.12:	The structure of Myoglobin containing a) a heme cofactor, b) 2 tryptophan (Trp) residues (Trp 7, Trp 14) and c) α -helices (A-G). 31
Figure 1.13:	The structure of BSA. 32
Figure 1.14:	PDB structure of HSA. 34
Figure 2.1:	Potential energy diagram of a diatomic molecule showing the different electronic energy states and their associated vibrational energy levels. 60
Figure 2.2:	Jablonski diagram, which illustrates other radiative and non-radiative processes that compete with fluorescence emission. 60

Figure 2.3:	Sketch of the detailed arrangement of TCSPC set up.	68
Figure 2.4:	The different components of TCSPC instrument; CFD (constant fraction discriminator), TAC (Time to Amplitude Converter), ADC (Analogue to Digital Converter).	73
Figure 2.5:	Sketch of the rotational anisotropy instrumentation.	80
Figure 2.6:	Sketch of the Dynamic Light Scattering (DLS) instrumentation.	86
Figure 3.1:	Temperature dependent fluorescence spectra of myoglobin (7 μ M) in (A) $w_0 = 4$, (B) Buffer (The thermal unfolding profile monitored at $\lambda_{em} = 350$ nm is shown in the inset). (C) Normalised thermal transition profile for Mb as a function of w_0 values monitored at $\lambda_{em} = 331$ nm. Temperature was varied from 10 $^{\circ}$ C to 90 $^{\circ}$ C for the reverse micelle samples.	99
Figure 3.2:	(A) CD spectra of Mb (7 μ M) in AOT/IO/H ₂ O(buffer) reverse micelles at different w_0 values and (B) Thermal denaturation profile of Myoglobin monitored at 222 nm in AOT/IO/H ₂ O(buffer) reverse micelle at $w_0 = 8$. The observed noncooperativity in the denaturation profile is conserved over a range of w_0 (= 4 and 12) values.	101
Figure 3.3:	CD spectra of Mb (14 μ M) in AOT/IO/H ₂ O(buffer) reverse micelles at $w_0 = 8$ containing different concentrations of urea (for the actual urea concentration refer to materials and methods). Shown in inset is the transition profile for Mb as a function of urea monitored at 222 nm.	103
Figure 3.4:	Fluorescence decay profiles of Mb in (A) AOT/IO/H ₂ O(buffer) reverse micelles as a function of different w_0 values and (B) buffer, with increase in concentration of urea. $\lambda_{exc} = 284$ nm and $\lambda_{em} = 330$ nm (for reverse micelle) and 360 nm (for buffer).	105
Figure 3.5:	Thermal denaturation of Mb in presence of (A) 0 M urea (B) 1 M urea, (C) 2 M urea, (D) 3 M urea, (E) 4 M Urea, (F) 5 M urea monitored at 222 nm using CD in presence of various crowding agents (200 g/L) as noted in the figure panels. The solid lines should just be regarded as aides to follow the transition. The concentration of Mb was 20 μ M for (A) while for the ones having urea, the protein concentration was kept at 25 μ M.	110
Figure 3.6:	Average lifetime ($\langle\tau\rangle$) plot of Mb as a function of urea in presence of (A) 100 g/L and (B) 200 g/L of various crowding agents.	114
Figure 4.1:	Far UV CD spectra of (a) HSA in buffer and at different w_0 values and (b) HSA in absence and presence of ANS in	138

	AOT/IO/H ₂ O(buffer) reverse micelles at $w_0 = 12$. ([HSA] = 2 μ M; [ANS] = 10 μ M, 20 μ M and 40 μ M for the 1:5, 1:10 and 1:20 systems respectively)	
Figure 4.2:	Thermal denaturation profile of HSA probed with ANS monitored at 222 nm in buffer and AOT/IO/H ₂ O(buffer) as function of w_0 values. Temperature was varied from 10 °C to 90 °C for all the samples. ([HSA] = 2 μ M and [ANS] = 2 μ M)	140
Figure 4.3:	Temperature dependent transition profile of HSA in buffer and HSA in AOT/IO/H ₂ O(buffer) at $w_0 = 12$ as mentioned in the figure legend using steady state fluorescence. ($\lambda_{exc} = 295$ nm; $\lambda_{em} = 340$ nm) ([HSA] = 2 μ M and [ANS] = 2 μ M)	144
Figure 4.4:	Normalized fluorescence spectra for HSA-ANS complexes in buffer and reverse micelle at $w_0 = 12$. $\lambda_{exc} = 350$ nm. ([HSA] = 5 μ M; [ANS] = 5 μ M and 25 μ M for the 1:1 and 1:5 systems respectively; for the ANS only samples, the respective concentrations have been mentioned in parentheses in the figure legend)	144
Figure 4.5:	A) Gaussian fit of the emission spectrum of ANS for HSA-ANS complex (1:1) excited at 375 nm for 10 °C showing the combination of bands used. B) Gaussian fits for the temperature dependent (10 °C to 50 °C) fluorescence spectra of ANS for the HSA-ANS (1:1) complex for $w_0 = 12$. $\lambda_{exc} = 350$ nm. ([HSA] = 2 μ M and [ANS] = 2 μ M)	146
Figure 4.6:	a) Spectra exhibiting FRET between Trp-214 and ANS in AOT/Isooctane/H ₂ O with increase in ANS concentration (10 μ M to 400 μ M) at $w_0 = 12$. $\lambda_{exc} = 295$ nm. b) Average fluorescence lifetime of HSA with increase in ANS concentration excited at 295 nm at different w_0 values. $\lambda_{em} = 330$ nm	151
Figure 4.7:	(a) Time resolved fluorescence decay curves for HSA-ANS in buffer and (b) Time resolved fluorescence decay curves for HSA-ANS (1:1) at $w_0 = 12$ for. Trp excitation ($\lambda_{exc} = 295$ nm) and ANS emission ($\lambda_{em} = 490$ nm) and for ANS excitation ($\lambda_{exc} = 375$ nm) and ANS emission ($\lambda_{em} = 490$ nm).	153
Figure 4.8:	Schematic representation of the proposed locations of ANS (red circles) based on the obtained rotational decay parameters in AOT reverse micelles. HSA, where present, has also been depicted as seen in the last two micelles for the two rows. The upper row is that of $w_0 = 12$ while the lower row shows the changes occurring in $w_0 = 8$. As depicted, on incorporation of HSA, the longer ANS	160

rotation component becomes smaller implying that this group of ANS molecules is drawn more towards the bulk portion of the water pool.

- Figure 5.1:** Representative Job's plots for determining the HSA-C153 binding stoichiometry in presence of different concentrations of Dextran 40. 174
- Figure 5.2:** Binding stoichiometry variation of BSA and HSA by Job's Plot method in presence of different crowding agents (a) Dextran 6 (b) Dextran 40 (c) Dextran 70 (d) Ficoll 70. (Representative Job's plot figures have been provided in SI Figures 5.1 and 5.2). 175
- Figure 5.3:** Variation of K_d as a function of crowder concentration (a) BSA-C153 complex in Dextran 6 (b) HSA-C153 complex in Dextran 6 (c) BSA-C153 in Dextran 70 complex (d) HSA-C153 complex in Dextran 70. 180
- Figure 5.4:** Dissociation constant profiles in presence of different concentrations of Dextran 40 for (a) BSA-Coumarin 153 complex (10 to 20 g/L) (b) BSA-Coumarin 153 complex (40 to 100 g/L) (c) HSA-Coumarin 153 complex (10 to 70 g/L) (d) HSA-Coumarin 153 complex (80 to 100 g/L) 182
- Figure 5.5:** Dissociation constant profiles in presence of different concentrations of Ficoll 70 for (a) BSA-Coumarin 153 complex (10 to 60 g/L) (b) BSA-Coumarin 153 complex (70 to 100 g/L) (c) HSA-Coumarin 153 complex. 183
- Figure 6.1:** Changes in integrated fluorescence intensity during chemical denaturation of HSA using urea: Trp emission from HSA excited at 295 nm in buffer and various crowding agents (a) in presence of Dextrans (b) in presence of PEGs. (HSA concentration = 5 μ M, Prodan concentration = 5 μ M) 196
- Figure 6.2:** Changes in integrated fluorescence intensity during chemical denaturation of HSA-Prodan using urea: (a) Trp emission from HSA-Prodan excited at 295 nm in buffer and various crowding agents (a) in presence of Dextrans (b) in presence of PEGs. (HSA concentration = 5 μ M, Prodan concentration = 5 μ M) 197
- Figure 6.3:** Fitted curves of Changes in integrated fluorescence intensity during chemical denaturation of HSA using Urea. (a) Trp emission from HSA excited at 295 nm in buffer. (b) Trp emission from HSA excited at 295 nm in 100 g/L Dextran 40. (c) Trp emission from HSA excited at 295 nm in 100 g/L Dextran 6. (d) Trp emission from HSA excited at 295 nm in 100 g/L PEG8000. 198

Figure 6.4:	Prodan emission from HSA-Prodan excited at 375 nm in buffer and various crowding agents. (HSA concentration = 5 μ M, Prodan concentration = 5 μ M)	204
Figure 6.5:	(a) Average life time of Prodan excitation at 466 nm of HSA-Prodan in presence of crowding agents with varying urea concentrations. (b) Average life time of Prodan excitation at 490 nm of HSA-Prodan in presence of crowding agents with varying urea concentrations. (c) Average life time of Prodan excitation at 520 nm of HSA-Prodan in presence of crowding agents with varying urea concentrations. (d) Normalized lifetime decays at 466 nm, 490 nm and 520 nm of HSA-Prodan in buffer excited at 375 nm. (HSA concentration = 2 μ M, Prodan concentration = 2 μ M)	209
Figure 6.6:	Rotational anisotropy decay of Prodan excitation of HSA-Prodan, probe at 466 nm with varying urea concentrations in buffer. (HSA concentration = 2 μ M, Prodan concentration = 2 μ M)	211
Figure 6.7:	Rotational time constant of faster component of Prodan of HSA-Prodan probe at 466 nm in presence of different crowding agents with varying urea concentrations.	211
SI Figure 3.1:	(A) Trend in fluorescence intensity of Mb (7 μ M) in AOT/H ₂ O/IO reverse micelle as a function of w_0 values. (B) Emission spectra of Myoglobin (5 μ M) in AOT/IO/H ₂ O(buffer) reverse micelle solution as a function of urea at $w_0 = 4$. Similar results were found for $w_0 = 8$ and $w_0 = 12$.	230
SI Figure 3.2:	Fluorescence decay traces of Mb with increase in urea concentration at $w_0 = 8$ ($\lambda_{exc} = 284$ nm and $\lambda_{em} = 330$ nm).	230
SI Figure 3.3:	Normalised thermal denaturation CD curves of Mb in presence of (A) 0 M urea (B) 3 M urea, (C) 4 M urea, (D) 5 M urea monitored at 222 nm using. The concentration of the various crowding agents used was 100 g/L. The solid lines should just be regarded as visual aides to follow the transition. The concentration of Mb was 20 μ M for (A) while for the ones having urea, the protein concentration was kept at 25 μ M.	231
SI Figure 3.4:	Urea induced denaturation of Mb (20 μ M) monitored using CD at 222nm in presence of various crowding agents of concentration (A) 100 g/L and (B) 200 g/L. The solid lines should just be regarded as visual aides to follow the transition.	232
SI Figure 3.5:	Fitted CD thermal denaturation curves (the empty circles are the raw data while the solid lines are the fits) of Mb in (A) buffer and (B) Ficoll 70 (200 g/L) as a function of urea concentration (as	232

	indicated).	
SI Figure 3.6:	Representative fluorescence decay traces of Mb with increasing urea concentration in presence of 200 g/L (A) Ficoll 70 and (B) Dextran 40 ($\lambda_{exc} = 284$ nm and $\lambda_{em} = 360$ nm). Y-axis has been represented in logarithmic units.	233
SI Figure 4.1:	(a) Far UV CD spectra of HSA in absence and presence of ANS in buffer. (b) Fluorescence emission spectra of NATA in reverse micelle.	241
SI Figure 4.2:	Thermal denaturation of HSA-ANS (1:1) complex in buffer excited at 375 nm.	241
SI Figure 4.3:	Thermal denaturation of HSA-ANS (a) 1:1 complex (b) 1:5 complex excited at 375 nm (c) Temperature dependence spectra of ANS same concentration as in HSA-ANS 1:1 (d) Temperature dependence spectra of ANS same concentration as in HSA-ANS 1:5 complex excited at 375 nm.	242
SI Figure 4.4:	Thermal denaturation of HSA-ANS (1:1) complex in buffer excited at 295 nm.	243
SI Figure 4.5:	(a) Overlap of absorption spectra of ANS with fluorescence spectra of HSA in buffer ($J(\lambda) = 6.04 \times 10^{13} \text{ nm}^4 \text{ M}^{-1} \text{ cm}^{-1}$). (b) Overlap of absorption spectra of ANS with fluorescence spectra of HSA at $w_0 = 12$.	243
SI Figure 4.6:	Representative anisotropy decays of ANS bound with HSA in buffer and in reverse micelle at $w_0 = 12$.	244
SI Figure 4.7:	Overlap of absorption spectra of C153 with fluorescence spectra of HSA at $w_0 = 12$.	244
SI Figure 4.8:	(a) Simulated decay profile of ANS in reverse micelle at $w_0 = 8$ and at $w_0 = 12$. (b) Simulated decay profile of C153 in reverse micelle at $w_0 = 8$ and at $w_0 = 12$.	244
SI Figure 5.1:	Job's plot analysis of HSA-Coumarin-153 binding in presence of increasing concentrations of various crowding agents.	245
SI Figure 5.2:	Job's plot analysis of HSA-Coumarin-153 binding in presence of increasing concentrations of various crowding agents.	246
SI Figure 5.3:	Representative Benesi-Hildebrand's plots for HSA-C153 complexes in presence of different crowding agents.	247
SI Figure 5.4:	Representative Benesi-Hildebrand's plots for BSA-C153 complexes in presence of different crowding agents.	248
SI Figure 6.1:	Fluorescence emission spectra of HSA-Prodan with increase in urea concentration excited at 295 nm in buffer.	261
SI Figure 6.2:	Fluorescence emission spectra of HSA-Prodan with increase in	261

	urea concentration excited at 375 nm in buffer.	
SI Figure 6.3:	Fluorescence emission spectra of HSA-Prodan with increase in urea concentration excited at 375 nm in Dextran 6.	262
SI Figure 6.4:	Fluorescence emission spectra of HSA-Prodan with increase in urea concentration excited at 375 nm in Dextran 40.	262
SI Figure 6.5:	Fluorescence emission spectra of HSA-Prodan with increase in urea concentration excited at 375 nm in Dextran 70.	263
SI Figure 6.6:	Fluorescence emission spectra of HSA-Prodan with increase in urea concentration excited at 375 nm in PEG200.	263
SI Figure 6.7:	Fluorescence emission spectra of HSA-Prodan with increase in urea concentration excited at 375 nm in PEG8000.	264
SI Figure 6.8:	Gaussian fit of the emission spectrum of Prodan for HSA-Prodan complex excited at 375 nm in buffer and in Dextran 6 at varying urea concentration.	265
SI Figure 6.9:	(a) Relative amplitudes of Gaussian fit of Prodan for HSA-Prodan complex excited at 375 nm in buffer and in different crowding agents at varying temperature monitored at (a) 520 nm and (b) 560 nm.	266

LIST OF TABLES

Table 3.1:	Fluorescence lifetime of Myoglobin in AOT/H ₂ O/IO reverse micelle as a function of w_0 (excited at 284 nm and emission was collected at 330 nm).	104
Table 3.2:	Fluorescence lifetime of Myoglobin in AOT/H ₂ O/IO reverse micelle as a function of urea (A) at $w_0 = 8$ (b) at $w_0 = 12$ (excited at 284 nm and emission was collected at 330 nm).	107
Table 3.3:	Values of T_m and ΔH_m of Myoglobin in buffer and Ficoll 70 in presence of varying concentrations of urea.	112
Table 3.4:	Fluorescence Lifetime (average) of Myoglobin as a function of urea in presence of various crowding agents (excited at 284 nm and emission was collected at 360 nm).	113
Table 4.1:	Summary of fluorescence lifetime measurements of HSA in AOT/Isooctane reverse micelles as a function of ANS concentration at different w_0 values (excited at 280 nm and probed at 340 nm).	149
Table 4.2:	FRET efficiencies (from time resolved data using equation 3) and D–A distances (r_{DA}) of HSA-ANS in AOT/Isooctane reverse micelles at different w_0 values.	155
Table 4.3:	Lifetime data of HSA and HSA-ANS (1:1) complex in buffer and reverse micelle $w_0= 12$.	156
Table 4.4:	Lifetime of HSA-ANS (1:5) ($\lambda_{exc} = 375$ nm) for $w_0 = 12$.	157
Table 4.5:	Rotational anisotropy decay parameters of HSA-ANS in AOT reverse micelle ($\lambda_{exc} = 375$ nm).	159
Table 5.1:	Dissociation constant (K_d) values for BSA-Coumarin 153 (BSA-C153) complex in presence of crowding agents.	176
Table 5.2:	Dissociation constant (K_d) values for HSA-Coumarin 153 (HSA-C153) complex in presence of crowding agents.	179
Table 6.1:	Thermodynamic parameters for Urea-induced unfolding of HSA.	199
Table 6.2:	FRET efficiency (E) in presence of crowding agents during chemical denaturation of urea. (Here we have used the area under the Trp emission to calculate E)	200
Table 6.3(a):	Time-resolved lifetime studies of Prodan within HSA-Prodan in buffer excited at 375 nm during chemical denaturation by urea.	206
Table 6.3(b):	Time-resolved lifetime studies of Prodan within HSA-Prodan excited at 375 nm in presence of Dextran 40 during chemical denaturation by urea.	207
Table 6.4(a):	Time-resolved anisotropy of Prodan within HSA-Prodan in buffer	210

	during chemical denaturation by urea measured at 466 nm.	
Table 6.4(b):	Time-resolved anisotropy of Prodan within HSA-Prodan in presence of Dextran 40 during chemical denaturation by urea.	210
SI Table 3.1:	Hydrodynamic diameter (D_H) of AOT reverse micelles without Mb and with Mb (8 μ M) with increase in urea concentration at $w_0 = 8$, T= 298 K respectively.	228
SI Table 3.2:	The physical parameters of the AOT/Isooctane reverse micelle environment.	228
SI Table 4.1:	The parameters for global Gaussian fitting for different temperatures in buffer for HSA-ANS (1:1) complex.	234
SI Table 4.2:	The parameters for global Gaussian fitting for different temperatures in $w_0 = 12$ for HSA-ANS (1:1) complex.	235
SI Table 4.3:	The parameters for global Gaussian fitting for different temperatures in $w_0 = 12$ HSA-ANS (1:5) complex.	237
SI Table 4.4a:	Theoretical efficiency in AOT/Isooctane reverse micelle environment.	238
SI Table 4.4b:	The physical parameters of the AOT/Isooctane reverse micelle environment.	239
SI Table 4.5:	Average life times of C153 in presence and absence of HSA in different medium (buffer as well as in AOT/Isooctane reverse micelle).	239
SI Table 4.6:	Rotational correlation time of C153 in presence and absence of HSA in different medium (buffer as well as in AOT/Isooctane reverse micelle).	240
SI Table 4.7:	By using Stoke's equation ($\tau_r = \frac{\eta V}{kT}$), we estimate the rotational time of the micelles of different sizes using the viscosity of isooctane ~ 0.5 cP.	240
SI Table 6.1:	Global Gaussian fitting of HSA-Prodan in presence of various crowding agents excited at 375 nm.	249
SI Table 6.2:	Time-resolved lifetime studies of Prodan within HSA-Prodan in PEG8000 excited at 375 nm during chemical denaturation by urea. (HSA concentration = 2 μ M, Prodan concentration = 2 μ M)	254
SI Table 6.3:	Time-resolved lifetime studies of Prodan within HSA-Prodan in PEG200 excited at 375 nm during chemical denaturation by urea. (HSA concentration = 2 μ M, Prodan concentration = 2 μ M)	255
SI Table 6.4:	Time-resolved lifetime studies of Prodan within HSA-Prodan in Dextran 6 excited at 375 nm during chemical denaturation by urea. (HSA concentration = 2 μ M, Prodan concentration = 2 μ M)	256

SI Table 6.5:	Time-resolved lifetime studies of Prodan within HSA-Prodan in Dextran 40 excited at 375 nm during chemical denaturation by urea. (HSA concentration = 2 μ M, Prodan concentration = 2 μ M)	257
SI Table 6.6:	Time-resolved lifetime studies of Prodan within HSA-Prodan in buffer excited at 375 nm during chemical denaturation by urea. (HSA concentration = 2 μ M, Prodan concentration = 2 μ M)	258
SI Table 6.7:	Time-resolved anisotropy of Prodan within HSA-Prodan in PEG8000 during chemical denaturation by urea measured at 466 nm. (HSA concentration = 2 μ M, Prodan concentration = 2 μ M)	259
SI Table 6.8:	Time-resolved anisotropy of Prodan within HSA-Prodan in PEG200 during chemical denaturation by urea measured at 466 nm. (HSA concentration = 2 μ M, Prodan concentration = 2 μ M)	259
SI Table 6.9:	Time-resolved anisotropy of Prodan within HSA-Prodan in Dextran 6 during chemical denaturation by urea measured at 466 nm. (HSA concentration = 2 μ M, Prodan concentration = 2 μ M)	260
SI Table 6.10:	Time-resolved anisotropy of Prodan within HSA-Prodan in Dextran 70 during chemical denaturation by urea measured at 466 nm. (HSA concentration = 2 μ M, Prodan concentration = 2 μ M)	260